2019 IEEE 16th International Symposium on Biomedical Imaging (ISBI 2019)
Venice, Italy, April 8-11, 2019

MULTI-SHELL DIFFUSION MRI MEASURES OF BRAIN AGING: A PRELIMINARY COMPARISON FROM ADNI3

Talia M. Nir[1], Sophia I. Thomopoulos[1], Julio E. Villalon-Reina[1], Artemis Zavaliangos-Petropulu[1], Emily L. Dennis[1], Robert I. Reid[2], Matt A. Bernstein[3], Bret Borowski[3], Clifford R. Jack, Jr.[3], Michael W. Weiner[4], Neda Jahanshad[1], Paul M. Thompson[1], for the Alzheimer's Disease Neuroimaging Initiative (ADNI)

[1] Imaging Genetics Center, Mark & Mary Stevens Neuroimaging & Informatics Institute, Keck School of Medicine, University of Southern California, Marina del Rey, CA.
[2] Department of Information Technology, Mayo Clinic and Foundation, Rochester, MN.
[3] Department of Radiology, Mayo Clinic and Foundation, Rochester, MN.
[4] Department of Radiology, University of California San Francisco School of Medicine, San Francisco, CA.

ABSTRACT

The Alzheimer's Disease Neuroimaging Initiative (phase 3; ADNI3) is collecting multisite diffusion MRI (dMRI) data using protocols optimized for different scanner vendors, including one multi-shell protocol, to better understand disease effects. Here, we analyzed multi-shell scans from 56 ADNI3 participants (age: 74.3±7.5 yrs; 17F/49M). We evaluated whether multi-shell dMRI measures computed from neurite orientation dispersion and density imaging (NODDI) and diffusion kurtosis imaging (DKI) differentiated people with mild cognitive impairment from healthy controls with higher sensitivity than standard diffusion tensor imaging (DTI) measures. We also assessed the effects of various multi-shell derived dMRI samples on the sensitivity of DTI measures. While we did not identify large differences in effect sizes among tensor-based, NODDI, or DKI measures, we did detect greater effect sizes from DTI measures estimated using multi-shell data converted to single-shell HARDI compared to those fit using the subset of 48 b=1000 s/mm^2 volumes, typical of DTI.

Index Terms— ADNI3, DTI, Multi-shell, NODDI, DKI

1. INTRODUCTION

The Alzheimer's Disease Neuroimaging Initiative (ADNI) is an ongoing multi-center, longitudinal study to improve methods for clinical trials by identifying brain imaging, clinical, cognitive, and molecular biomarkers of AD and aging. In particular, identifying biomarkers sensitive to mild cognitive impairment (MCI) is important to better categorize the transitional stages between normal aging and AD, and to evaluate targeted treatments. To date, amyloid and tau biomarkers from CSF and PET, are perhaps the most widely accepted biomarkers of AD and MCI for epidemiological, genetic studies, and for clinical trials. Still, there is growing interest in diffusion (dMRI) measures, which offer additional sensitivity to microstructural properties not evident on standard anatomical MRI.

The first phase of ADNI acquired dMRI data from approximately one third of enrolled participants on GE scanners. In its third phase, ADNI3 has incorporated dMRI protocols for 3T Siemens, Philips, and GE scanners to allow dMRI data collection at all sites. The available scanners span a wide range of software capabilities, such as support for custom diffusion gradient tables and/or simultaneous multi-slice acceleration. Including additional scanners in ADNI3, while accommodating scanner restrictions and limiting scan duration to 7-10 minutes, resulted in data acquired with 7 different acquisition protocols (http://adni.loni.usc.edu/methods/documents/mri-protocols).

Of the seven protocols, there is currently only one multi-shell protocol —for sites with Siemens Advanced Prisma scanners. Several AD-related studies have already used multi-shell protocols to compute diffusion measures from models that do not assume mono-exponential decay, such as diffusion kurtosis imaging (DKI) [1, 2], and multi-compartment models such as neurite orientation dispersion and density imaging (NODDI) [3, 4]. Such multi-shell biophysical and advanced signal based models of water diffusion in brain tissue may allow us to relate diffusion signals directly to underlying microstructure and resolve multiple dominant fiber directions, potentially offering greater specificity and sensitivity to disease processes.

Multi-shell scans are now available for 56 of over 600 scanned ADNI3 participants. To boost power and pool data across all ADNI3 protocols and participants, single-shell models need to be evaluated. The single-tensor model (DTI) [5] is still the most widely used to detect alterations in white matter (WM) micro-architecture in clinical populations, despite known limitations in regions with crossing fibers and the lack of specificity to characterize microstructural environments. For DTI, the optimal b-value lies between

b=900-1200 s/mm^2 [6, 7], and at least 30 unique sampling orientations are recommended to robustly estimate anisotropy, mean diffusivity, and tensor orientations [8]. Frequently, such studies use simulations or phantom data, which are subject to different sources of noise than human clinical data and may not be directly comparable. In practice, including sampling orientations from the other shells may help boost the signal to noise ratio (SNR), improving sensitivity to disease related effects. One recent approach, proposed by Ye et al. (2016), converts multi-shell data to single-shell high angular resolution diffusion imaging (HARDI). In [9], diffusion signals and dMRI measures from the converted data were highly correlated with those collected from a true HARDI acquisition. The clinical utility of this method, however, has not yet been evaluated.

Here, we analyzed dMRI data from 56 ADNI3 participants scanned with a multi-shell protocol to evaluate the sensitivity of various microstructural measures to detect differences between cognitively normal (CN) elderly individuals and those with MCI. We hypothesized that multi-shell dMRI measures derived from NODDI and DKI models would confer higher sensitivity than DTI, and that DTI measure effects sizes would depend on how multi-shell data are used for single tensor estimation— i.e., using a subset of b-values, the entire acquisition, or conversion to HARDI as in [9].

2. METHODS

2.1. Subjects and Image Acquisition

Baseline MRI, dMRI, diagnosis, and demographic data were downloaded from the ADNI database (https://ida.loni.usc.edu/). Here we analyzed data from the 56 participants scanned with a multi-shell dMRI protocol: 39 cognitively normal elderly controls (CN; mean age: 73.2±7.2 yrs; 25M/14F) and 17 with mild cognitive impairment (MCI; mean age: 76.8±7.5 yrs; 14M/3F). (Data collection for the study is ongoing, and this constitutes an initial report.)

All subjects underwent whole-brain MRI scanning on 3T Siemens Advanced Prisma scanners at 9 acquisition sites across North America. Anatomical T1-weighted MPRAGE sequences (256x256 matrix; voxel size = 1.0x1.0x1.0 mm; TI=900 ms; TR = 2300 ms; TE = 2.98 ms; flip angle=9°), and multi-shell multiband dMRI (116x116 matrix; voxel size: 2x2x2 mm; TR=3400 ms; scan time = 7.25 min) were collected. 127 separate images were acquired for each dMRI scan: 13 b_0 images, 48 b=1000 s/mm^2 diffusion-weighted images (DWI), 6 b=500 s/mm^2 DWI, and 60 b=2000 s/mm^2 DWI.

For comparison with dMRI measures, hippocampal volume measures, processed by the UCSF team using the FreeSurfer package pipeline [10], were also downloaded from the ADNI database.

2.2 Image Preprocessing

DWI images were denoised using the LPCA filter [11] and corrected for Gibbs ringing with MRtrix [12]. Extra-cerebral tissue was removed, and eddy correction performed with FSL's *EDDY* tool [13] including *repol* outlier replacement [14]. DWI then underwent B1 field inhomogeneity corrections [15]. T1-weighted images were preprocessed using the standard FreeSurfer pipeline [10]. Corrected b_0 images were linearly aligned to resulting FreeSurfer corrected T1 images, using the WM mask for FSL *FLIRT's* boundary-based registration (BBR) [16]; the registration was subsequently inverted to bring the T1 to the native DWI space. Diffusion images were then non-linearly warped to their respective T1-weighted scans with ANTs [17] to correct for EPI-induced susceptibility artifacts. Diffusion gradient directions were rotated to account for linear registrations.

2.3 dMRI Reconstruction Models and Scalar Measures

Fractional anisotropy (FA_{1000}) and mean diffusivity (MD_{1000}) were estimated by fitting a single diffusion tensor (DTI) [5] to the subset of 48 b=1000 s/mm^2 DWI volumes. To compare performance with a measure derived from a HARDI technique—non-parametric q-ball imaging (QBI)—we also fit constant solid angle orientation distribution functions (CSA-ODFs) [18, 19] using the DiPy package [20] to generate generalized FA (GFA_{1000}) maps.

Two multi-shell models were fit across all shells. Three diffusion kurtosis imaging (DKI) [1] measures were estimated using the DiPy package: axial kurtosis (AK), radial kurtosis (RK), and mean kurtosis (MK). Neurite orientation dispersion and density imaging (NODDI) [3] was fit using the AMICO toolbox [21] yielding maps of the orientation dispersion index (ODI), intra-cellular volume fraction (ICVF), and isotropic volume fraction (ISOVF).

2.3 Multi-shell Samples for Single-shell Measures

For comparison with measures derived from the subset of 48 b=1000 s/mm^2 DWI volumes, DTI and QBI CSA-ODFs were subsequently fit to the full multi-shell dMRI acquisition with b=500, 1000, and 2000 s/mm^2 and FA_{ALL}, MD_{ALL} and GFA_{ALL} maps estimated.

Additionally, multi-shell dMRI were interpolated into corresponding single-shell HARDI using the generalized q-sampling method (GQI) framework proposed in [9], available through DSI Studio. The GQI model provides a linear relation between dMRI signal and the diffusing spins via a spin density function (SDF; [22]), consequently enabling a direct conversion between spins and dMRI signals acquired from shell or grid sampling schemes. Here, multi-shell data were converted to single-shell HARDI data with b=1000 s/mm^2 and again FA_{HARDI}, MD_{HARDI} and GFA_{HARDI} maps were generated.

2.5 White Matter Region of Interest Measures

Using publically available ENIGMA-DTI protocols (http://enigma.usc.edu/protocols/dti-protocols/) [23], each subject's FA map was warped to the ENIGMA-DTI FA template with ANTs [17] and the transformations applied to all respective dMRI scalar maps. DTI, QBI, DKI and NODDI measures were projected onto the ENIGMA-DTI template skeleton with TBSS [24]. Using the JHU WM atlas [25], mean skeletonized measures were extracted from 25 regions of interest (ROIs; **Table 1**).

Table 1. Index of 25 JHU atlas WM ROIs analyzed.

CST	Corticospinal tract	**FX**	Fornix (body)
IC	Internal capsule	**SLF**	Sup. longitudinal fasciculus
ALIC	Ant. limb of IC	**SFO**	Sup. fronto-occipital fasciculus
PLIC	Post. limb of IC	**IFO**	Inf. fronto-occipital fasciculus
RLIC	Retrolenticular part of IC	**SS**	Sagittal *stratum*
PTR	Post. thalamic radiation	**Fx/ST**	Fornix *(crus)/Stria terminalis*
CR	*Corona radiata*	**UNC**	Uncinate fasciculus
ACR	Ant. *corona radiata*	**CC**	Full corpus callosum
SCR	Sup. *corona radiata*	**GCC**	Genu of CC
PCR	Post.*corona radiata*	**BCC**	Body of CC
CGC	Cingulum (cingulate)	**SCC**	Splenium of CC
CGH	Cingulum (hippocampal)	**Full WM**	Full white matter
EC	External capsule		

2.6 Statistical Analyses

Random-effects linear regressions were used to test for associations between MCI diagnosis and mean dMRI measures in each ROI or hippocampal volume, covarying for age, sex and their interaction, and grouping the data by acquisition site. Effect sizes were estimated with Cohen's *d*. The false discovery rate (FDR) procedure was used to correct for multiple comparisons across ROIs (q=0.05)[26].

3. RESULTS

3.1 Multi-shell versus Single-shell dMRI Measures

Compared to CN participants, the MCI group showed significantly lower FA_{1000}, GFA_{1000}, AK, RK, MK, and ICVF, and higher MD_{1000} (FDR q<0.05; **Figure 1**). No significant associations were detected with ODI. The largest effect size across measures and ROIs was detected with MD in the Full WM (d = 1.72). Except for ISOVF, every measure significantly associated with MCI included the Full WM ROI (**Figure 2**). For those measures where the Full WM was significant, secondary analyses tested for significant regional associations when the Full WM was included as an additional covariate. Except for a now positive association between ICVF in the body of the corpus callosum (BCC) and MCI (i.e., less "neuronal loss" in the BCC than the rest of the WM), ROI associations were no longer significant indicating that no regional effect differed significantly from the global effect detected in the Full WM. dMRI effect sizes in the Full WM exceeded those detected with hippocampal volume in the same subjects (d = -0.95).

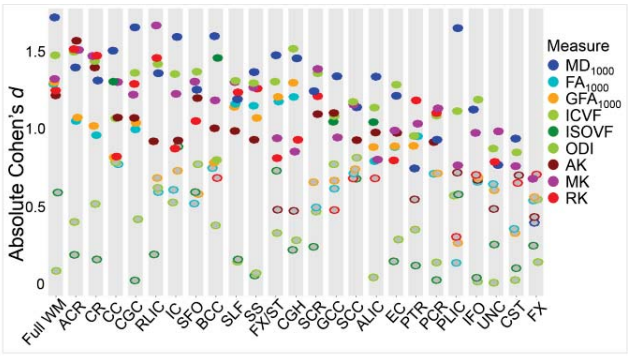

Figure 1. Absolute value of effect sizes for associations between MCI diagnosis and single or multi-shell dMRI measures from the DTI (*blue colors*), QBI (*orange*), DKI (*reds*) and NODDI (*greens*) models. Significant associations (FDR q<0.05) are indicated by filled circles.

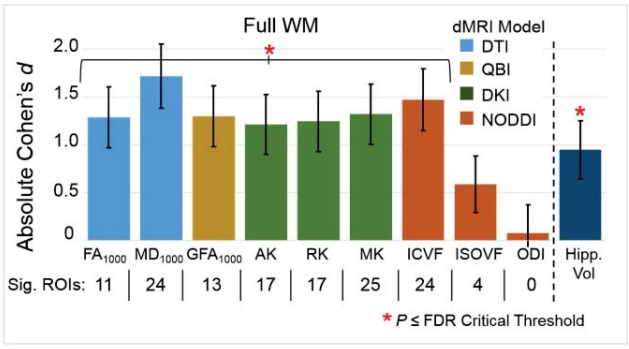

Figure 2. Absolute value of effect sizes (and standard error bars) for associations between MCI diagnosis and dMRI measures in the Full WM; the effect size for hippocampal volume (mean of left and right) is shown for comparison. For each measure, the total number of ROIs significantly associated with diagnosis is also noted, as a measure of the extent of effects (we note that this is just a heuristic as it depends on the available sample size).

3.2 Single-shell Measures from Multi-shell Data

MD_{1000}, MD_{ALL}, and MD_{HARDI} all showed significant associations in 24 of 25 ROIs (FDR q<0.05), and effect sizes were comparable (within the standard error). FA_{1000} and FA_{ALL} showed similar effect sizes, and were significantly associated with 11 and 9 ROIs respectively. FA_{HARDI}, like MD, was significantly associated with MCI diagnosis in 24 ROIs and showed larger effect sizes (**Figure 3A**). Similarly, GFA_{1000} and GFA_{ALL} showed similar effect sizes, and were significantly associated with diagnosis in 13 and 11 ROIs respectively, but GFA_{HARDI} was associated with diagnosis in 22 ROIs and again offered larger effect sizes (**Figure 3B**).

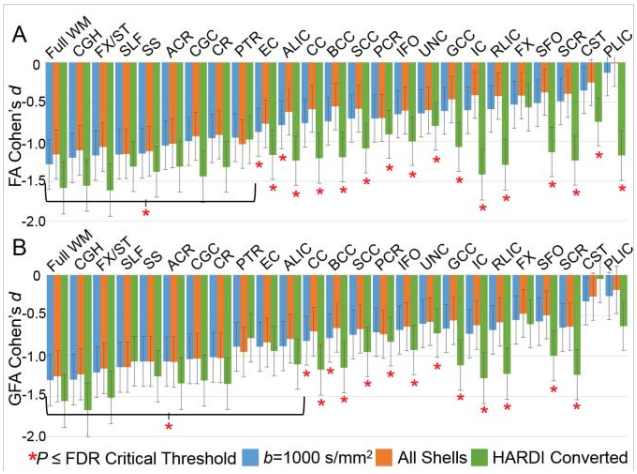

Figure 3. Effect sizes (and standard error bars) for associations between MCI diagnosis and **(A)** DTI or **(B)** QBI derived fractional anisotropy measures.

5. DISCUSSION

This study has three main findings: 1) Compared to DKI and NODDI multi-shell measures, DTI MD in the Full WM showed similar if not larger effect sizes for detecting differences between CN and MCI diagnostic groups; 2) dMRI measure effect sizes exceeded those detected with hippocampal volume, a more standard anatomical measure of aging and AD; 3) Compared to single-shell measures fit on only the subset of 48 b=1000 s/mm^2 sampling directions, more pervasive associations with larger effect sizes were detected for QBI GFA and DTI FA when fit to multi-shell data converted to single-shell HARDI.

DTI is widely used to study neurodegenerative disorders such as AD; lower FA and higher MD are still the most frequently reported dMRI measures in studies of AD. The DTI model, however, cannot differentiate crossing fibers, and captures partial volumes of different tissue compartments (e.g., intra- and extra-cellular compartments, 'free water' from CSF or inflammation, and myelin volume fraction). This may reduce the sensitivity and specificity of single tensor measures. While multi-shell models such as DKI and NODDI may overcome some of these limitations, data from clinical studies, including most sites in ADNI3, may be limited to single-shell acquisitions, constraining the available models to simpler models such as DTI. A number of AD-related pathological processes are thought to drive changes in DTI measures including demyelination and axonal degeneration, gliosis, neuro-inflammation and swelling [27]. Biophysical models such as NODDI may offer greater insight into underlying pathology (e.g., in our study, higher MD in the Full WM detected in MCI may in part be driven by neuronal loss indicated by lower ICVF, the second largest Full WM effect size detected). Even so, our findings so far suggest that similar if not greater effect sizes to distinguish patient groups (i.e., MCI vs. CN) may be obtained with DTI measures, perhaps because they collapse all pathological changes in the WM under a Gaussian modeling frame. There are, however, several implementations of NODDI (e.g., NODDI Toobox [28] and Dmipy [29]), and further comparisons are necessary. In addition, future work should focus on the ICVF, with which the second largest Full WM effect size was detected. Here, as in the original NODDI model, the 'Stick' model [30] was used, but several other intra-axonal diffusion models have been proposed [31-32].

In multi-site studies such as ADNI3, where data from single and multi-shell dMRI are combined or compared, the question remains how best to use multi-shell data for fitting mono-exponential models such as QBI and DTI. While theoretically it may suffice to fit DTI with 30 volumes with b=1000 s/mm^2, we found that converting full multi-shell acquisitions to single-shell HARDI data using the framework proposed by Yeh et al. (2016) improved sensitivity to detect disease related effects; the largest anisotropy effect sizes were detected with the multi-shell data when it was converted to HARDI. GFA_{HARDI} and FA_{HARDI} detected the largest effect sizes in the hippocampal cingulum and fornix (crus) / *stria terminalis* region (followed by the full WM), WM bundles connecting hippocampal and parahippocampal regions to the rest of the brain, consistent with patterns of AD pathology.

As ADNI3 progresses and sample sizes grow, future studies are needed to verify which measures offer greater diagnostic sensitivity and microstructural interpretability.

5. ACKNOWLEDGMENTS

Data collection and sharing for ADNI was funded by NIH grant U01 AG024904 and DOD award W81XWH-12-2-0012. Additional support was provided by NIA grant RF1 AG04191 and P41 EB015922.

6. REFERENCES

[1] J.H. Jensen, et al., "Diffusional kurtosis imaging: the quantification of non-gaussian water diffusion by means of magnetic resonance imaging," *Magn Reson Med*, vol. 53, no. 6, pp. 1432-40, 2005.

[2] L. Yuan, et al., "Non-Gaussian diffusion alterations on diffusion kurtosis imaging in patients with early Alzheimer's disease," *Neurosci Lett*, vol. 616, pp. 11-8, 2016.

[3] H. Zhang, et al., "NODDI: practical in vivo neurite orientation dispersion and density imaging of the human brain," *NeuroImage*, vol. 61, no. 4, pp. 1000-16, 2012.

[4] N. Colgan, et al., "Application of neurite orientation dispersion and density imaging (NODDI) to a tau pathology model of Alzheimer's disease," *NeuroImage*, vol. 125, pp. 739-744, 2016.

[5] P.J. Basser, et al., "MR diffusion tensor spectroscopy and imaging," *Biophys J*, vol. 66, no. 1, pp. 259-67, 1994.

[6] D.C. Alexander and G.J. Barker, "Optimal imaging parameters for fiber-orientation estimation in diffusion MRI," *NeuroImage*, vol. 27, no. 2, pp. 357-67, 2005.

[7] P.B. Kingsley and W.G. Monahan, "Selection of the optimum b factor for diffusion-weighted magnetic resonance imaging assessment of ischemic stroke," *Magn Reson Med*, vol. 51, no. 5, pp. 996-1001, 2004.

[8] D.K. Jones, "The effect of gradient sampling schemes on measures derived from diffusion tensor MRI: a Monte Carlo study," *Magn Reson Med*, vol. 51, no. 4, pp. 807-15, 2004.

[9] F.C. Yeh and T.D. Verstynen, "Converting Multi-Shell and Diffusion Spectrum Imaging to High Angular Resolution Diffusion Imaging," *Frontiers in Neuroscience*, vol. 10, pp. 418, 2016.

[10] B. Fischl, et al., "Automatically parcellating the human cerebral cortex," *Cereb Cortex*, vol. 14, pp. 11-22, 2004.

[11] J.V. Manjon, et al., "Diffusion weighted image denoising using overcomplete local PCA," *PLoS One*, vol. 8, no. 9, pp. e73021, 2013.

[12] E. Kellner, et al., "Gibbs-ringing artifact removal based on local subvoxel-shifts," *Magn Reson Med*, vol. 76, no. 5, pp. 1574-1581, 2016.

[13] J.L.R. Andersson and S.N. Sotiropoulos, "An integrated approach to correction for off-resonance effects and subject movement in diffusion MR imaging," *NeuroImage*, vol. 125, pp. 1063-1078, 2016.

[14] J.L.R. Andersson, et al., "Incorporating outlier detection and replacement into a non-parametric framework for movement and distortion correction of diffusion MR images," *NeuroImage*, vol. 141, pp. 556-572, 2016.

[15] N.J. Tustison, et al., "N4ITK: improved N3 bias correction," *IEEE Trans Med Imaging*, vol. 29, no. 6, pp. 1310-20, 2010.

[16] D.N. Greve and B. Fischl, "Accurate and robust brain image alignment using boundary-based registration," *NeuroImage*, vol. 48, no. 1, pp. 63-72, 2009.

[17] B.B. Avants, et al., "A reproducible evaluation of ANTs similarity metric performance in brain image registration," *NeuroImage*, vol. 54, no. 3, pp. 2033-44, 2011.

[18] D.S. Tuch, "Q-ball imaging," *Magn Reson Med*, vol. 52, no. 6, pp. 1358-72, 2004.

[19] I. Aganj, et al., "Reconstruction of the orientation distribution function in single- and multiple-shell q-ball imaging within constant solid angle," *Magn Reson Med*, vol. 64, no. 2, pp. 554-66, 2010.

[20] E. Garyfallidis, et al., "Dipy, a library for the analysis of diffusion MRI data," *Front Neuroinform*, vol. 8, pp. 8, 2014.

[21] A. Daducci, et al., "Accelerated Microstructure Imaging via Convex Optimization (AMICO) from diffusion MRI data," *Neuroimage*, vol. 105, pp. 32-44, 2015.

[22] F.C. Yeh et al., "Generalized q-sampling imaging," *IEEE Trans Med Imaging*, vol. 29, no. 9, pp. 1626-35, 2010.

[23] N. Jahanshad, et al., "Multi-site genetic analysis of diffusion images and voxelwise heritability analysis: a pilot project of the ENIGMA-DTI working group," *Neuroimage*, vol. 81, pp. 455-469, 2013.

[24] S.M. Smith, et al., "Tract-based spatial statistics: voxelwise analysis of multi-subject diffusion data," *NeuroImage*, vol. 31, no. 4, pp. 1487-505, 2006.

[25] S. Mori, et al., "Stereotaxic white matter atlas based on diffusion tensor imaging in an ICBM template," *Neuroimage*, vol. 40, no. 2, pp. 570-582, 2008.

[26] Y. Benjamini and Y. Hochberg, "Controlling the false discovery rate- a practical and powerful approach to multiple testing," *Journal of the Royal Statistical Society Series B-Methodological*, vol. 57, no. 1, pp. 289-300, 1995.

[27] C. Laurent et al., "Tau and neuroinflammation: What impact for Alzheimer's Disease and Tauopathies?," *Biomedical Journal*, vol. 41, no. 1, pp. 21-33, 2018.

[28] P. Coupe, et al., "An optimized blockwise nonlocal means denoising filter for 3-D magnetic resonance images," *IEEE Trans Med Imaging*, vol. 27, no. 4, pp. 425-41, 2008.

[29] D.F. Tate, et al., "Regional areas and widths of the midsagittal corpus callosum among HIV-infected patients on stable antiretroviral therapies," *J Neurovirol*, vol. 17, no. 4, pp. 368-79, 2011.

[30] T.E. Behrens, et al., "Characterization and propagation of uncertainty in diffusion-weighted MR imaging," *Magn Reson Med*, vol. 50, no. 5, pp. 1077-88, 2003.

[31] O. Söderman and B. Jönsson, "Restricted Diffusion in Cylindrical Geometry," *Journal of Magnetic Resonance*, vol. 117, no. 1, pp. 94-97, 1995.

[32] P.T. Callaghan, "Pulsed-Gradient Spin-Echo NMR for Planar, Cylindrical, and Spherical Pores under Conditions of Wall Relaxation," *Journal of Magnetic Resonance, Series A*, vol. 113, no. 1, pp. 53-59, 1995.